Enhancing Human-Robot Collaborative Transportation through Obstacle-Aware Vibrotactile Warning and Virtual Fixtures

Doganay Sirintuna[1,a,b,*], Theodora Kastritsi[1,a], Idil Ozdamar[1,a,b], Juan M. Gandarias[c] and Arash Ajoudani[a]

[a]Human-Robot Interfaces and Interaction Laboratory, Istituto Italiano di Tecnologia, Via San Quiricio 19d, Genoa, 16163, Italy
[b]Dept. of Informatics, Bioengineering, Robotics, and System Engineering, University of Genoa, Via All'Opera Pia 13, Genoa, 16145, Italy
[c]Robotics and Mechatronics, Systems Engineering and Automation Department, University of Malaga, Calle Dr Ortiz Ramos, Malaga, 29010, Spain

ARTICLE INFO

Keywords:
Human-Robot Co-transportation
Mobile Manipulation
Vibrotactile Feedback
Virtual Fixture

ABSTRACT

Transporting large and heavy objects can benefit from Human-Robot Collaboration (HRC), increasing the contribution of robots to our daily tasks and addressing challenges arising from labor shortages. This strategy typically positions the human collaborator as the leader, with the robot assuming the follower role. However, when transporting large objects, the operator's situational awareness can be compromised as the objects may occlude different parts of the environment, weakening the human leader's decision-making capacity and leading to failure due to collision. This paper proposes a situational awareness framework for collaborative transportation to face this challenge. The framework integrates a multi-modal haptic-based Obstacle Feedback Module with two units. The first unit consists of a warning module that alerts the operator through a haptic belt with four vibrotactile devices that provide feedback about the location and proximity of the obstacles. The second unit implements virtual fixtures as hard constraints for mobility. The warning feedback and the virtual fixtures act online based on the information given by two Lidars mounted on a mobile manipulator to detect the obstacles in the surroundings. By enhancing the operator's awareness of the environment, the proposed module improves the safety of the human-robot team in collaborative transportation scenarios by preventing collisions. Experiments with 16 non-expert subjects in four feedback modalities during four scenarios report an objective evaluation thanks to quantitative metrics and subjective evaluations based on user-level experiences. The results reveal the strengths and weaknesses of the implemented feedback modalities while providing solid evidence of the increased situational awareness of the operator when the two haptic units are employed.

1. Introduction

Collaborative robots have recently reached remarkable advancements, enabling safe operation alongside humans without physical barriers. These human-robot partnerships, leveraging human cognitive skills in conjunction with the precision and repeatability of robots, offer tremendous potential as high-performance solutions across various sectors, with significant implications for manufacturing, logistics, and industrial settings [1].

Existing Human-Robot Collaboration (HRC) approaches in the literature have mainly focused on understanding human intentions and designing robotic systems to respond accordingly to establish an intuitive collaboration similar to a human-human partnership. Recent research studies have shown that effective human-robot teams can provide real practical solutions in diverse domains, including assembly [2], surface treatment [3], and sawing [4].

However, the application of intuitive and bi-directional communication must also be considered, as it increases the human operator's situational awareness about the current state of the task and the environment to increase safety and efficiency [5]. Various communication interfaces have been explored depending on the specific work environments, tasks, and information types. For instance, in [6, 7, 8], augmented reality (AR) interfaces were employed to inform the human operator about different phases of a collaborative task. In another study [9], a graphical user interface (GUI) was used to operate a configurable set of robotic arms, providing the human operator with information about active robots, selected control strategies, and options to reconfigure the robots according to the task requirements. Similarly, Merlo et al. [10] displayed a (GUI) on a screen to instruct human users on their assigned roles during a collaborative

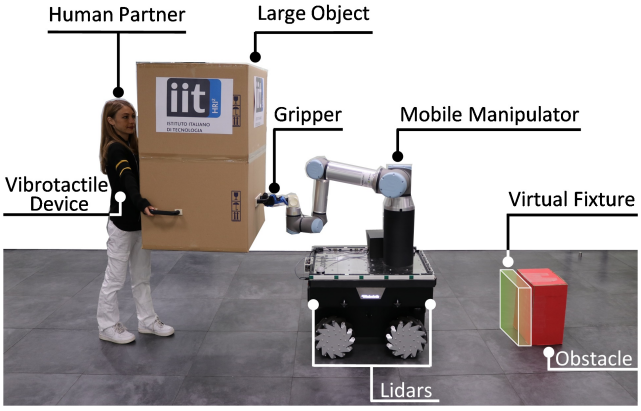

Fig. 1: We propose a novel multi-modal feedback module based on vibrotactile feedback and virtual fixtures to augment the operator's awareness of the environment during collaborative transportation.

*Corresponding author
[1]These authors contributed equally to this work.

assembly task. As an alternative to visual interfaces, verbal feedback has been investigated to increase human situational awareness during collaborative tasks [11].

A standard task in industrial settings involves transporting bulky objects. This dyadic task usually demands high physical effort and requires adaptability to the surroundings. Collaborative mobile manipulators can work synergistically with humans to conduct seamlessly such activities. Nevertheless, as mobility introduces safety considerations due to collision[2], the communication between robots and humans assumes a pivotal role in enhancing situational awareness, thus emphasizing its substantive significance. Despite this necessity, the problem of situational awareness in dyadic mobile collaborative tasks has not been faced systematically. Considering the nature of the task, it is not feasible to employ many of the interaction interfaces used in the literature, including the examples above, to provide feedback to the human operator. While the visual interfaces are impractical due to the mobility of the task, the approaches that utilize verbal feedback may not be suitable for noisy environments, such as manufacturing sites.

In this paper, we propose a novel situational awareness framework applied to a collaborative carrying task. This framework incorporates a multi-modal haptic-based Obstacle Feedback Module that combines a Vibrotactile Warning Unit and a Virtual Fixture Unit to inform the human operator about the obstacles in the environment (see Fig. 1). The framework is not only capable of informing the human operator about obstacles in the environment but also restricting the underlying motion when necessary. In our previous work [12], we introduced a promising solution for co-carrying of bulky, deformable, and ungraspable objects where the transportation task is purely led by the human. That approach, however, focused on the human-robot interaction regarding co-transportation, assuming that no obstacles were present in the environment. This assumption limits the application potential of the solution and demotes safety in real workplaces. In addition, as the experiments reveal in [12], the human field of view can be limited when carrying large objects, potentially jeopardizing safety and increasing the probability of operational setbacks. To overcome these limitations, this study presents the following contributions:

- Development of a multi-modal haptic-based situational awareness framework that augments the operators' perception of the environment. This framework is integrated into our human-robot co-transportation system [12], that features a whole-body interaction controller and planner for a mobile collaborative robot. The goal is to use the robot's onboard sensors to scan the environment and to provide feedback to the leader human (hence, not interfering with the leader-follower dynamics), and to reduce the likelihood of operational setbacks.
- Development of a Vibrotactile Warning Unit using the ErgoTac-Belt [13]. This unit provides information about the location and the distance of the nearby obstacles. Hence, even if an operator cannot see an obstacle (see Fig. 1), his/her spatial awareness is augmented thanks to this unit and the robot's onboard sensory system.
- Design and implementation of a Virtual Fixture Unit to constraint the motion of a mobile manipulator in pHRI tasks using Lidars' data. When the human-robot dyad reaches an obstacle despite the vibrotactile warning, this unit adjusts the robot's end-effector desired velocity in order to: i) prevent collisions with obstacles, and ii) give the user a sense of resistance when moving against them (kinesthetic feedback).
- Experimentation and validation of the proposed methodology in an industrial-like co-transportation task. The methodology has been evaluated under different conditions with multiple subjects. In particular, 16 subjects carried out a task with a real robot in four different environments with four different modalities: no feedback, only vibrotactile warning, only virtual fixtures, and multi-modal modality combining vibrotactile warning and virtual fixtures. Both quantitative metrics and qualitative evaluations through usability and workload questionnaires are presented in this article. Results are reported, and an overall discussion of the significant advances and limitations of the proposed framework about the applicability in actual manufacturing and logistics environments and a comparison with the state-of-the-art are included.

Although human-robot co-transportation is a widely researched topic in HRC literature, to the best of the authors' knowledge, no prior study has focused on augmenting the operator's awareness to avoid collisions with the surroundings, especially for scenarios where the human leader's decision-making capability is compromised. The novelty of our approach that faces this challenge lies in its multi-model haptic feedback module. While the Virtual Fixture Unit utilizes the 2D Lidar data of the mobile platform to constrain the motion of the team led by the human operator, differing from the previous approaches that focus on (semi)autonomous obstacle avoidance of mobile robots, the vibrotactile devices are used for the first time to convey information about the location and proximity of the obstacles in the HRC literature.

The rest of the article is structured as follows: The following section summarizes the most relevant state-of-the-art works on the previously mentioned topics: Human-robot collaborative transportation, Virtual fixtures, and Vibrotactile devices. Section 3 presents the proposed framework. Section 4 describes the experiments and how the overall

[2]Standard and autonomous collision avoidance algorithms can be ineffective in such scenarios due to the complex nature of manufacturing environments that are dynamically changing and hard to model/adapt. Hence, humans must have the leading role and be able to dynamically adjust the behavior of the dyadic system.

evaluation of the framework is conducted. The results and a discussion of the contributions, advantages, and limitations in the context of the state-of-the-art are presented in Section 5. Finally, we conclude the study with possible future directions in Section 6.

2. Related Work

2.1. Human-Robot Collaborative Transportation

In the field of physical Human-Robot Interaction (pHRI), the concept of transportation of jointly held objects is an appealing use case as it leverages the complementary skills offered by humans and robots. During this physically challenging task, the cognitive abilities of the human bring the required adaptability to the team for the unstructured environment of manufacturing sites, while the robot partner assists the human by sharing the load.

In recent research, there has been a considerable focus on examining how robots can proactively assist humans in carrying objects instead of a mere follower role. In [14], active assistance of the robot during collaborative manipulation is achieved by employing a learning framework based on Programming by Demonstration (PbD). During kinesthetic teaching, the required position and the compliance constraints for the interaction controller are encoded. In a similar work [15], the proposed PbD approach, which can adjust the leader and follower behavior distribution, is validated through a 1-D collaborative lifting task. Alternatively, Bussy et al. proposed a proactive control scheme that exploits anticipated human motion intention based on pre-defined velocity thresholds [16, 17]. Building upon this framework, researchers extended their controller by including visual information in the co-transportation of a rigid table while ensuring that a ball remains on top of it [18].

Although the previously mentioned proactive approaches reduce the non-gravitational load which is required to guide the robot during the intended trajectory, the human partners still prefer to be the leader while collaborating [19]. In addition, the complex nature of manufacturing environments makes it challenging to utilize pre-trained models and heuristic-based proactive approaches, as these methods struggle to adapt to dynamic changes that frequently occur in such sites. For instance, an adaptive impedance controller is introduced to enhance the transparency of the physical collaboration in [20, 21]. Here, the damping parameter of the controller is adjusted according to the human acceleration/deceleration intention. In [22], a collaborative carrying framework, where the robot follows the human-induced motion as a follower during the transportation of a rigid table, is implemented by exploiting the compliance of the arms of the humanoid robot. As an alternative, we proposed an adaptive object deformation-agnostic framework for human-robot collaborative transportation in our previous study [23]. The presented framework combines the human kinematic information with the haptic information transferred through the object to generate reactive whole-body movements on the robot partner. Later, this framework is extended to collaborate with multiple robot partners to handle bulky objects which cannot be effectively manipulated by a single robot partner [12].

2.2. Virtual Fixtures

In HRI applications that require high cognitive demand, partial knowledge of the task is often utilized. This task knowledge might involve a desired estimated motion, a desired known analytical path, restricted regions presented as point clouds, or a desired trajectory learned through demonstration. To leverage this partial knowledge and enhance HRI performance in terms of safety, precision, and reduced cognitive load for the user, researchers have employed a constraint control method known as active constraints (AC)/virtual fixtures (VF) control. The concept of AC/VF originated in tele-robotic manipulation, where Rosenberg introduced force feedback from virtual environments to ease the cognitive burden on the user [24, 25]. Since then, AC/VF techniques have found applications in various domains, including surgical procedures, industrial tasks, and underwater robotics. The adoption of virtual fixtures can be considered as a specialized application of shared control [26].

VF can be classified as virtual fixtures intended for establishing boundaries around restricted areas or virtual fixtures meant to aid in directing towards a desired path; notice that, a guidance virtual fixture in a particular region can be considered as a forbidden-region virtual fixture for its corresponding complementary space, and vice versa. An extensive survey on VF can be found in [27], which highlights various approaches for their enforcement. Certain methods utilize constraint quadratic optimization techniques [28, 29], albeit at the expense of computational demands and potential inconsistencies among constraints and cost functions [27]. Alternatively, some methods use controllers that do not store energy [30, 31, 32] while others employ energy storage methods like artificial potential fields (AP) [33, 34, 35, 36, 37]. To the best of the authors' knowledge, in the existing literature on mobile platforms, numerous works delve into obstacle avoidance; however, these primarily address autonomous [38] or semi-autonomous operations in a teleoperation setup [39], leaving aside physical human-robot interaction tasks such as co-transportation, which is the focus of the present work.

2.3. Vibrotactile Devices

The use of warning/feedback devices [40, 41] in industrial scenarios has been considered a feasible solution to some of the most known challenges in the industry, such as the reduction of Work-related Musculoskeletal Disorders (WMDs) [42]. One of the main advantages of these devices is the underlying cost-profit trade-off.

While other feedback modalities are not recommended in industrial workplaces due to several issues, such as the distraction caused by staring at the screens in visual feedback [43, 44], the high levels of occupational noise in audio feedback systems [45], or the discomfort in prolonged industrial operations due to the applied mechanical pressure

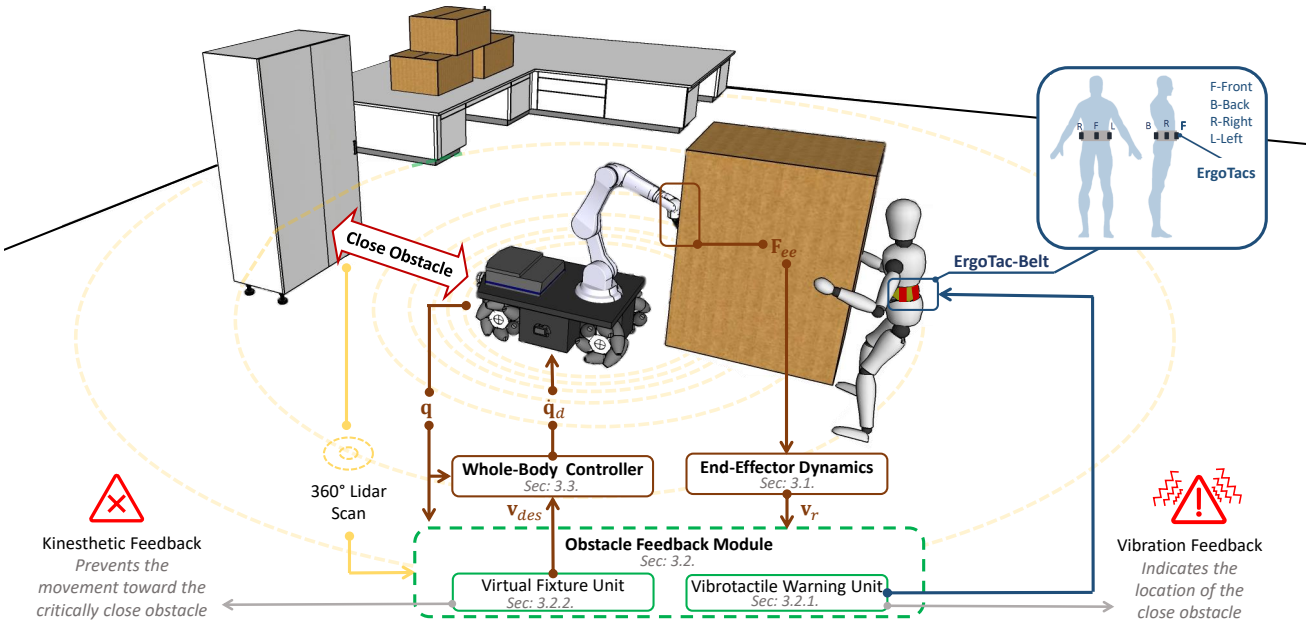

Fig. 2: High-level scheme of the proposed framework. The *Obstacle Feedback Module* aims to augment the human awareness of obstacles in the vicinity detected by the robot's sensory systems. While the *Vibrotactile Warning Unit* produces vibratory feedback to the human through an ErgoTac-Belt indicating the detected obstacle's location and proximity, the *Virtual Fixture Unit* prevents physical contact between the human-robot team and the environment by restricting the end-effector velocity obtained from the *End-Effector Dynamics* when a critically close obstacle is present. Lastly, the *Whole-Body Controller* calculates the required joint velocities for the mobile platform based on the desired end-effector velocity.

in mechano-tactile feedback devices [46, 47], wearable vibrotactile devices is a promising alternative as they do not jeopardize human senses.

At the same time, they are a viable choice in contrast to bulky and heavy wearable systems that become unpractical when the task demands a certain amount of mobility. In addition, vibrotactile feedback seems to be a profitable option regarding familiarization with the device and the feedback modality [48]. The use of this technology to improve users' awareness in HRI [49], balance control [50], prosthetic control [47], posture optimization [51], and teleoperation [52] have already shown promising results.

In our previous work [53], we presented ErgoTac, a wearable device that uses vibration feedback to improve human ergonomics when performing heavy industrial tasks. Performance analysis of ErgoTac in comparison with another haptic-based wearable feedback device is described in [54]. Later, we used ErgoTac-Belt, which employs four of the same devices, to guide the user based on the human center of pressure while walking [13]. Moreover, these kinds of tactile interfaces are also employed in the literature for human-robot teams. For example, Casalino et al. employed a vibrotactile ring to convey information to the user regarding the state of a collaborative assembly task [55].

3. Proposed Framework

The interconnections between hardware and software components of our interactive co-transportation framework are shown in Fig. 2. The employed robotic platform, which has a manipulator attached on top of its base, is driven by omnidirectional wheels that allow the platform to avoid non-holonomic constraints yielding movements over a large workspace. It is equipped with an anthropomorphic robotic hand attached to the end-effector to co-carry objects with the human partner, a Force/Torque sensor at the flange to measure the wrenches resulting from the interaction, and Lidars for inspecting the surroundings to detect obstacles.

The proposed framework can be subdivided into three operational components, namely the *End-Effector Dynamics*, the *Obstacle Feedback Module*, and the *Whole-Body Controller*. The first one calculates a reference velocity following a standard admittance control law given in Sec. 3.1 based on the force transferred through the object. The *Obstacle Feedback Module* aims to augment the human partner's sensations and yields awareness of the obstacles outside the field of view alongside the visible ones by making use of its *Vibrotactile Warning* and *Virtual Fixture Units*. The first unit starts to generate warning vibrations via ErgoTac-Belt [13] for conveying information about the location and proximity of the obstacles before the human-robot team gets dangerously close to any of them. On the other hand, the latter restricts the team's movement in the direction of the potential collision but only when the distance to the obstacle becomes critically low. Lastly, the *Whole-Body Controller* generates required joint velocities for the robotic platform using the desired velocity obtained from the *Obstacle Feedback Module*.

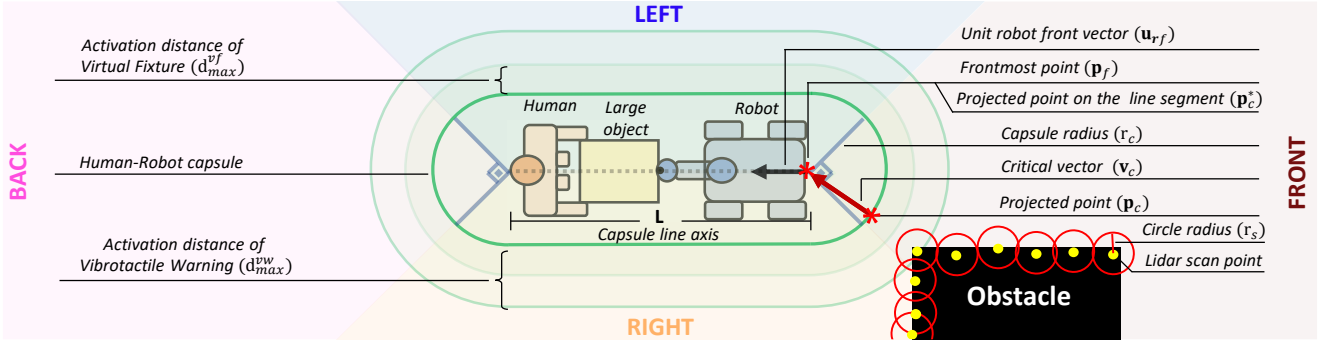

Fig. 3: Illustration of the capsule with length L and radius r_c encompassing the human, the robot, and the object in between. The activation distances of *Virtual Fixture* and *Vibrotactile Warning Units* are denoted by d^{vf}_{max} and d^{vw}_{max}, respectively. The center of the red circles corresponds to the Lidar scan points, and the radius of the circles (r_s) is chosen to be large enough to ensure effective coverage of the gaps between the Lidar points. The $\mathbf{p}_c$ indicates the point on the capsule that is nearest to making contact with one of the circles. The $\mathbf{p}^*_c$ refers to the point on the line segment closest to $\mathbf{p}_c$, while $\mathbf{p}_f$ represents the frontmost point of the human-robot team, which coincides with $\mathbf{p}^*_c$ based on the given obstacle localization. Finally, the critical and the unit robot front vectors are denoted as $\mathbf{v}_c$ and $\mathbf{u}_{rf}$, where they point from $\mathbf{p}_c$ to $\mathbf{p}^*_c$, and $\mathbf{p}_f$ to the human partner, respectively.

3.1. End-Effector Dynamics

In order to acquire the desired dynamic behavior of the robot's end-effector in Cartesian translational space, a mass-damper model is employed as follows:

$$\mathbf{M}_{ee}\dot{\mathbf{v}}_{ee} + \mathbf{D}_{ee}\mathbf{v}_{ee} = \mathbf{F}_{ee}, \tag{1}$$

where $\mathbf{v}_{ee} \in \mathbb{R}^3$ is the desired translational velocity of the end-effector, $\mathbf{M}_{ee}$ and $\mathbf{D}_{ee} \in \mathbb{R}^{3\times3}$ are constant positive defines matrices of the inertia and damping respectively, and $\mathbf{F}_{ee} \in \mathbb{R}^3$ is the measured forces exerted at the robot end-effector.

To ensure safety and prevent the robot from surpassing its operational limits, the output velocity is saturated with a unit slope as follows:

$$\mathbf{v}_r = \begin{cases} \mathbf{v}_{ee}, & \text{if } ||\mathbf{v}_{ee}|| \le v_{max} \\ v_{max}\dfrac{\mathbf{v}_{ee}}{||\mathbf{v}_{ee}||}, & \text{else} \end{cases}, \tag{2}$$

where $v_{max} \in \mathbb{R}_{>0}$ is the maximum allowed velocity magnitude (the saturation limit) and $\mathbf{v}_r \in \mathbb{R}^3$ is the resultant velocity after applying saturation.

3.2. Obstacle Feedback Module

Our goal is to prevent any physical contact between the human-robot team and the surfaces of objects in the surrounding environment in order to achieve protection for both. These surfaces are represented by a finite set of points from the 2D Lidar data of the mobile platform, denoted as $\mathcal{O}_l \subset \mathbb{R}^2$. To fill the empty spaces resulting from this representation, we create circles $C(\mathbf{p}_i; r_s)$ in the x-y plane of the Lidars, each with a radius $r_s \in \mathbb{R}_{\ge0}$, centered at the point $\mathbf{p}_i \in \mathcal{O}_l$. This approach is inspired by [37], where spheres were used instead of circles to fill the empty space resulting from the representation of sensitive organs using a 3D point cloud.

In this work, we consider that the human and robot are rigidly connected via the object being carried where their initial relative configuration remains fixed throughout the interaction. Additionally, we assume that there is minimal change of the end-effector frame w.r.t. the base frame of the mobile platform. Thus, the human-robot team can be enclosed within a capsule shape, defined by a line segment with length $L \in \mathbb{R}_{\ge0}$ and radius $r_c \in \mathbb{R}_{\ge0}$ (see Fig. 3). Consequently, the objective of preventing physical contact between the human-robot team and the surrounding environment is achieved if the capsule does not touch the perimeter of the overlapping circles.

Let $\mathbf{p}_f \in \mathbb{R}^2$ represent the position of the frontmost point of the human-robot team projected onto the x-y plane of the Lidars, and $\mathbf{u}_{rf} \in \mathbb{R}^2$ being the unit robot front vector pointing from $\mathbf{p}_f$ towards the human (see Fig. 3). This vector aligns with the negative x-axis of the mobile platform's base frame. Utilizing this information, we can determine the axis of the capsule line in the x-y plane of the Lidars that encompasses the human-robot team as follows:

$$\mathbf{p}_l(\sigma) = \mathbf{p}_f + \mathbf{u}_{rf}L\sigma \quad \in \mathbb{R}^2, \tag{3}$$

where $\sigma \in [0, 1]$ specifies the position along the axis of the capsule.

Within each control cycle, and for all points $\mathbf{p}_i$ belonging to the set $\mathcal{O}_l$, the nearest point on the line segment of the capsule is found by $\mathbf{p}^*_i = \mathbf{p}_l(\sigma^*_i)$ where σ^*_i can be found analytically [56]:

$$\sigma^*_i = \begin{cases} \zeta_i, & \text{if } 0 \le \zeta_i \le 1 \\ 1, & \text{if } \zeta_i > 1 \\ 0, & \text{if } \zeta_i < 0 \end{cases}, \ \zeta_i = \frac{1}{L}\mathbf{u}^{\mathrm{T}}_{rf}(\mathbf{p}_i - \mathbf{p}_f) \in \mathbb{R} \tag{4}$$

where the operator $(...)^{\mathrm{T}}$ symbolises the transpose of a vector/matrix. Then the resulting closest point on the perimeter of the capsule is calculated by:

$$\mathbf{p}^c_i = \mathbf{p}^*_i + \frac{\mathbf{p}_i - \mathbf{p}^*_i}{||\mathbf{p}_i - \mathbf{p}^*_i||}r_c. \tag{5}$$

To exclude the human user and the carried object from consideration and focus only on the nearest obstacles within a distance $\mathrm{d}_{max} \in \mathbb{R}_{>0}$, we define the set:

$$\mathcal{O}_o = \{\mathbf{p}_i \in \mathcal{O}_l \,:\, 0 < d_{xi} < \mathrm{d}_{max}\}, \tag{6}$$

where $d_{xi} \in \mathbb{R}$ represents the distance between the capsule and the circle $C(\mathbf{p}_i; \mathrm{r}_s)$, and it is given by:

$$d_{xi} = ||\mathbf{p}_i - \mathbf{p}_i^*|| - (\mathrm{r}_c + \mathrm{r}_s). \tag{7}$$

When the set $\mathcal{O}_o$ is not empty, in order to have a smooth reaction, instead of taking into account only the nearest point of the point cloud with respect to the capsule, we opt to represent all the closest points on the capsule perimeter of the $\mathbf{p}_i \in \mathcal{O}_o$ by a single point. To give more influence to the closest points, the represented point is determined through a weighted calculation as follows:

$$\bar{\mathbf{p}} = \frac{\sum_{\mathbf{p}_i \in \mathcal{O}_o} w_i \mathbf{p}_i^c}{\sum_{\mathbf{p}_i \in \mathcal{O}_o} w_i} \in \mathbb{R}^2, \tag{8}$$

where $w_i \in \mathbb{R}_{>0}$ represents the weights. These weights are exponentially inverse proportional with the distances between the circles $C(\mathbf{p}_i; \mathrm{r}_s)$ and the capsule as follow:

$$w_i = exp(-\alpha d_{xi}), \tag{9}$$

where $\alpha \in \mathbb{R}_{>0}$ is a scalar gain. By doing so, we ensure that the resulting point is profoundly influenced by its nearest neighbors. Since the average point $\bar{\mathbf{p}}$ may not lie within the capsule perimeter, we project this point onto the capsule surface as follows:

$$\mathbf{p}_c = \bar{\mathbf{p}}^* + \frac{\bar{\mathbf{p}} - \bar{\mathbf{p}}^*}{||\bar{\mathbf{p}} - \bar{\mathbf{p}}^*||}\mathrm{r}_c \quad \in \mathbb{R}^2, \tag{10}$$

where $\bar{\mathbf{p}}^*$ is the nearest point on the line segment of the capsule to the point $\bar{\mathbf{p}}$, which is calculated by utilizing (3) and (4) substituting $\mathbf{p}_i$ with $\bar{\mathbf{p}}$. The respective critical vector $\mathbf{v}_c \in \mathbb{R}^2$, depending on whether the set $\mathcal{O}_o$ is empty or not, is given by:

$$\mathbf{v}_c = \begin{cases} \dfrac{\mathbf{p}_c^* - \mathbf{p}_c}{||\mathbf{p}_c^* - \mathbf{p}_c||} & \mathcal{O}_o \neq \emptyset \\ \mathbf{0}_{2\times 1} & \text{else} \end{cases}, \tag{11}$$

where $\mathbf{p}_c^*$ is the nearest point on the line segment of the capsule to the point $\mathbf{p}_c$, which is calculated by utilizing (3) and (4) substituting $\mathbf{p}_i$ with $\mathbf{p}_c$. It is worth noting that when the projected velocity of the robot's end-effector in the x-y plane forms an obtuse angle with the critical vector $\mathbf{v}_c$, it indicates that the human-robot team is moving towards the nearest obstacles.

In this work, we utilized the distances d_{xi} and the critical vector $\mathbf{v}_c$ to determine the proximity of the human-robot team to the obstacles and the likelihood of collisions between them. To mitigate this potential danger, we propose implementing two layers of feedback reactions that are activated at different distances denoted as d_{max}^{vw} and d_{max}^{vf} (see Sec. 3.2.1 and Sec. 3.2.2). The first layer comprises a warning system that notifies the human via vibrotactile vibrations. The second layer imposes limitations on the motion of the human-robot team, preventing any contact with the obstacles, which also serves as kinesthetic feedback to the user.

3.2.1. Vibrotactile Warning Unit

This module aims to alert the human operator about the closeness and the location of obstacles in the vicinity using the Ergotac-Belt, which consists of 4 vibrotactile feedback devices representing the body relative directions (see Fig. 2). This module is enabled when an obstacle is at a distance smaller than $\mathrm{d}_{max}^{vw} \in \mathbb{R}_{>0}$ from the human-robot team capsule. In such cases, we calculate the critical vector $\mathbf{v}_c^{vw}$, as given by (11), based on the set $\mathcal{O}_o^{vw}$ from (6), substituting d_{max} with d_{max}^{vw}.

In this work, we decided not to vibrate more than one vibrotactile device simultaneously, as in our previous study [13], in order to avoid the cognitive burden of the human operator. Therefore, we generate warnings only for the nearest object by exploiting $-\mathbf{v}_c^{vw}$. As depicted in Fig. 3, the angle between $-\mathbf{v}_c^{vw}$ and $\mathbf{u}_{rf}$ is represented by $\theta_{\mathbf{u}_{rf}}^{\mathbf{v}_c^{vw}}$ that indicates the region in which includes the closest points in the vicinity. Each region can be represented by two border angles, θ^{b_1} and θ^{b_2}, with a consistent 90-degree difference between these across all four regions. The warnings are regulated to prevent fluctuations between different ErgoTacs when the nearest object is close to the border of the two adjacent areas. To do so, we enabled switching to a new vibrotactile feedback device if only the $\theta_{\mathbf{u}_{rf}}^{\mathbf{v}_c^{vw}}$ has deviated from the border angles of the previously warned region by a specified threshold, denoted as θ_{th}.

Moreover, the intensity of the vibrations is adjusted based on the minimum distance between the circles $C(\mathbf{p}_i; \mathrm{r}_s)$ and the capsule. This distance can be derived as:

$$\mathrm{d}_{obs} = \min_{\mathbf{p}_i \in \mathcal{O}_o^{vw}} \{d_{xi}\}, \tag{12}$$

where d_{xi} is given by Eq. (7). In particular, the intensity of the vibration is determined by the following rule:

$$I_t = \begin{cases} 1 & \mathrm{d}_{obs} \leq \mathrm{d}_{crit} \\ 1 - \frac{\mathrm{d}_{obs} - \mathrm{d}_{crit}}{\mathrm{d}_{max}^{vw} - \mathrm{d}_{crit}} & \mathrm{d}_{crit} < \mathrm{d}_{obs} \leq \mathrm{d}_{max}^{vw}. \end{cases} \tag{13}$$

This rule adjusts the intensity of warning vibrations as a linear function of the distance d_{obs}. The maximum intensity is achieved at a critical distance ($\mathrm{d}_{crit} < \mathrm{d}_{max}^{vw}$), while the minimum occurs at the maximum distance (d_{max}^{vw}).

For clarity, the pseudocode for selecting the region (R_t) to be vibrated associated with the appropriate ErgoTac device and the intensity of the vibrations (I_t) is given in Algorithm 1.

Algorithm 1 Obstacle-Aware Vibrotactile Warning

Input: $R_{t-1}, \mathcal{O}_o^{vw}, RobotOdometry$
Output: R_t, I_t
  $\mathrm{d}_{obs} \leftarrow getMinimumDistance$ ▷ Eq. (12)
  if $\mathrm{d}_{obs} > \mathrm{d}_{max}^{vw}$ **then**
    $R_t \leftarrow None$
    $I_t \leftarrow 0$
  else
    $\mathbf{v}_c^{vw} \leftarrow getCriticalVector$ ▷ Eq. (11)
    $\mathbf{u}_{rf} \leftarrow getUnitRobotFrontVector$
    $\theta_{\mathbf{u}_{rf}}^{\mathbf{v}_c^{vw}} \leftarrow getAngleBetween(-\mathbf{v}_c^{vw}, \mathbf{u}_{rf})$
    $R^* \leftarrow getRegion(\theta_{\mathbf{u}_{rf}}^{\mathbf{v}_c^{vw}})$
    if R^* equal to R_{t-1} **then**
      $R_t \leftarrow R^*$
    else
      $(\theta^{b_1}, \theta^{b_2}) \leftarrow getBorderAngles(R_{t-1})$
      if $min\{|\theta_{\mathbf{u}_{rf}}^{\mathbf{v}_c^{vw}} - \theta^{b_1}|, |\theta_{\mathbf{u}_{rf}}^{\mathbf{v}_c^{vw}} - \theta^{b_2}| > \theta_{th}\}$ **then**
        $R_t \leftarrow R^*$ ▷ Switch
      else
        $R_t \leftarrow R_{t-1}$ ▷ No Switch
      end if
      $I_t \leftarrow computeIntensity(\mathrm{d}_{obs})$ ▷ Eq. (13)
    end if
  end if

3.2.2. Virtual Fixture Unit

This module is enabled when the human-robot team is dangerously close to obstacles, i.e., when there is at least one circle $C(\mathbf{p}_i; \mathrm{r}_s)$ that is at a distance smaller to $\mathrm{d}_{max}^{vf} \in \mathbb{R}_{>0}$ from the human-robot team capsule, where $\mathrm{d}_{max}^{vf} < \mathrm{d}_{max}^{vw}$. In this case, the critical vector $\mathbf{v}_c^{vf} \in \mathbb{R}^2$, given by (11), is calculated based on the set $\mathcal{O}_o^{vf} \subset \mathcal{O}_l$ given by (6), with d_{max} substituted by d_{max}^{vf}. When the set $\mathcal{O}_o^{vf}$ is not empty, our objective is to stop the motion of the human-robot team when the projected velocity of the end-effector $\mathbf{v}_{r_{xy}} = \mathbf{v}_{r\{1:2\}} \in \mathbb{R}^2$ forms an obtuse angle with the critical vector $\mathbf{v}_c^{vf}$, i.e., when $\mathbf{v}_{r_{xy}}{}^{\mathrm{T}}\mathbf{v}_c^{vf} < 0$, as this indicates that the human-robot team is moving towards the obstacles.

To achieve this, we calculate the desired end-effector velocity as follows:

$$\mathbf{v}_{des} = (1 - b)\mathbf{v}_r \quad \in \mathbb{R}^2, \tag{14}$$

where $\mathbf{v}_r$, given by (2), represents the resultant velocity obtained after applying the saturation function to the desired velocity and $b \in \mathbb{R}$ is a function that takes values between zero and one. This function is utilized to determine whether to allow or restrict the resultant velocity based on the potential collision. To ensure a smooth reaction, we design this function as a dynamic system:

$$\dot{b} = f(b, \mathbf{v}_c^{vf}, \mathbf{v}_r). \tag{15}$$

This approach allows continuous adjustment of the variable b in response to changes in the desired end-effector velocity ($\mathbf{v}_{des}$) and the resultant velocity ($\mathbf{v}_r$).

To achieve quick and smooth responses, in this work, we choose the following function:

$$f(b, \mathbf{v}_c^{vf}, \mathbf{v}_r) = -\mathrm{a}_x\big(b - \beta(\mathbf{v}_c^{vf}, \mathbf{v}_r)\big), \tag{16}$$

which provides an exponential response to the b variable, where $\mathrm{a}_x \in \mathbb{R}_{>0}$ is a gain that indicates how rapidly the exponential function decays and $\beta \in \mathbb{R}$ is given by:

$$\beta(\mathbf{v}_c^{vf}, \mathbf{v}_r) = \begin{cases} 0, & \text{if} \quad \mathbf{v}_{r_{xy}}{}^{\mathrm{T}}\mathbf{v}_c^{vf} \geq 0 \\ 1, & \text{else} \end{cases}. \tag{17}$$

This step function serves as an indicator of the activation of the virtual fixture enforcement. It's important to note that the variable b tends exponentially towards β. Therefore, when the constraint is activated ($\beta = 1$), the commanded velocity tends towards zero. In order to ensure that the human-robot team will never touch the obstacles, the gain a_x must be carefully selected based on the maximum Cartesian velocity produced by the *End-Effector Dynamics* (v_{max}) and the distance d_{max}^{vf}. Specifically, the following condition must hold true:

$$\mathrm{a}_x > \frac{\mathrm{v}_{max}}{\mathrm{d}_{max}^{vf}}. \tag{18}$$

This condition can be easily proved by calculating the solution of (15) for b and then taking the integral of (14).

Alternatively, another way to design b can be by using the function $f(\mathbf{v}_c^{vf}, \mathbf{v}_r) = -\gamma a_x$, and then constraining b to move within the [0, 1] range, with γ given by:

$$\gamma(\mathbf{v}_c^{vf}, \mathbf{v}_r) = \begin{cases} -1, & \text{if} \quad \mathbf{v}_{r_{xy}}{}^{\mathrm{T}}\mathbf{v}_c^{vf} \geq 0 \\ 1, & \text{else} \end{cases}. \tag{19}$$

In this way, the desired end-effector velocity can be set exactly to zero.

3.3. Whole-Body Controller

In this study, a $(\mathrm{n}_b + \mathrm{n}_a)$-DoF mobile manipulator is controlled using a weighted whole-body damped least-squares inverse kinematics controller, where the base and arm have n_b and n_a degrees of freedom, respectively. This scheme calculates the desired joint velocities $\dot{\mathbf{q}}_d \in \mathbb{R}^{\mathrm{n}_b+\mathrm{n}_a}$ resulting in the desired end-effector while exploiting the redundancy of the robot as the secondary task. The primary cost function that is implemented to track the desired end-effector velocity is expressed as:

$$\mathcal{L}_1 = ||\dot{\mathbf{x}}_r - \mathbf{J}\dot{\mathbf{q}}||^2_{\mathbf{W}_1} + ||k\dot{\mathbf{q}}||^2_{\mathbf{W}_2}, \tag{20}$$

where $\dot{\mathbf{x}}_r = [\mathbf{v}_{des}^{\mathrm{T}} \ \mathbf{v}_{r_{\{3\}}} \ \mathbf{0}_{1\times3}]^{\mathrm{T}} \in \mathbb{R}^6$ is the desired twist of the end-effector, $\mathbf{v}_{r_{\{3\}}}$ represents the velocity in the z-axis resulting from the end-effector dynamics after saturation, $\mathbf{J} \in \mathbb{R}^{6\times(\mathrm{n}_b+\mathrm{n}_a)}$ is the whole-body robotic Jacobian, $\mathbf{W}_1 \in \mathbb{R}^{6\times6}$ and $\mathbf{W}_2 \in \mathbb{R}^{(\mathrm{n}_b+\mathrm{n}_a)\times(\mathrm{n}_b+\mathrm{n}_a)}$ are diagonal positive definite matrices and $k \in \mathbb{R}_{>0}$ is the so-called damping factor [57], which depends on the manipulability index of the arm to avoid kinematic singularities [58, 59, 60].

The secondary task that keeps the arm close to the initial configuration is formulated as the following cost function:

$$\mathcal{L}_2 = ||\mathbf{q}_{init} - \mathbf{q}||^2_{\mathbf{W}_3}, \tag{21}$$

where $\mathbf{q}_{init}$ is the initial joint configuration and $\mathbf{W}_3 = diag\{\mathbf{0}_{\mathrm{n}_b}, \zeta \mathbf{1}_{\mathrm{n}_a}\} \in \mathbb{R}^{(\mathrm{n}_b+\mathrm{n}_a)\times(\mathrm{n}_b+\mathrm{n}_a)}$ is a diagonal positive semidefinite matrix with ζ being the null-space gain. The desired joint velocities, which minimize this secondary cost function, are calculated as the negative gradient of it projected onto the null-space of the first task. A detailed explanation of this whole-body controller can be found in our previous work [61].

4. EXPERIMENTS

The experiments were designed to evaluate the effectiveness of the units in the *Obstacle Feedback Module*, as in the absence of the feedback they provided, the operator would be unable to navigate to the target location without encountering any collisions. To this end, the participants were asked to co-carry an object until they reached the finish line that was located 2.8 m ahead of their initial point, where they were unaware of the positions of obstacles placed in the environment. The videos of these experiments with an additional demonstration where the operator aimed to reach the target line while the position of an obstacle was dynamically changed are available at https://youtu.be/BRvDC8XLOWM.

4.1. Experimental Setup

In the experiments, the Kairos mobile manipulator is employed as the robotic platform for executing the co-transportation task with the human partner. It comprises an Omni-directional Robotnik SUMMIT-XL STEEL mobile base, a high payload 6-DoFs Universal Robot UR16e arm with an F/T sensor to measure the applied wrenches at the robot's flange, a Pisa/IIT Softhand gripper, and two 2D SICK Microscan Lidar sensors. These sensors are located at the back and front of the robot base and 30 cm above the ground, providing a 360-degree sensing range. The ErgoTac-Belt is composed of 4 ErgoTac units located at the front (F), right (R), left (L), and back (B) of the operator at the L5 level (see Fig. 2). At the user side, robust and pleasant vibration feedbacks are generated thanks to ErgoTac's small dimension (68.1 mm × 37.0 mm × 17.3 mm), lightweight (28 g), and wireless communication feature with low energy consumption (multi-point connection via Bluetooth low energy at 2.4 GHz).

The values of the parameters for the proposed framework utilized in the experiments are outlined in Table 1. As the experiments were carried out in the x-y plane, the mass and damping parameters of the z-axis were deliberately set to high values to avoid movements along the z-axis. The length (L) and the radius (r_c) of the capsule were selected large enough to encompass the human, the mobile robot, and the object in between, which is a 4.7 kg box with dimensions of $80 \times 60 \times 105$ cm (see Fig. 1). The co-carried object was intentionally chosen such that it would obscure a substantial portion of the human's frontal and peripheral vision, making it challenging for the participants to see most of the surroundings. Moreover, d^{vf}_{max} was selected to be equal to $\mathrm{d}_{\mathrm{crit}}$. This equivalence is attributed to the aim of achieving the highest level of vibration when the constraint unit is enabled. The choice of values for the parameters a_x, v_{max}, and d^{vf}_{max} was specifically designed to uphold the validity of condition (18) which ensure that no collision will occur. Furthermore, the chosen parameters of the whole-body controller leveraged the locomotion behavior of the mobile robot, where the relative arm configuration w.r.t to the base was kept almost the same throughout the task.

Table 1
Value of parameters used in the experimental setup

End-Effector Dynamics (Sec. 3.1)	
Parameter	**Value**
$\boldsymbol{M}_{ee}$	$diag\{40, 20, 50\}$
$\mathbf{D}_{ee}$	$diag\{90, 50, 1000\}$
v_{max}	0.5
Obstacle Feedback Module (Sec. 3.2)	
Parameter	**Value**
L	2.3
r_c	0.5
r_s	0.02
α	100
Vibrotactile Warning Unit (Sec. 3.2.1)	
Parameter	**Value**
θ_{th}	5
d^{vw}_{max}	0.6
d_{crit}	0.25
Virtual Fixture Unit (Sec. 3.2.2)	
Parameter	**Value**
d^{vf}_{max}	0.25
a_x	8
Whole-Body Controller (Sec. 3.3)	
Parameter	**Value**
n_a	6
n_b	3
$\mathbf{W}_1$	$diag\{1000_{1x3}, 500_{1x3}\}$
$\mathbf{W}_2$	$diag\{\mathbf{5}_{n_b}, \mathbf{2}_{n_a}\}$
ζ	3

4.2. Experimental Procedure

The co-transportation experiments have been conducted using 4 different feedback modalities, which are the combinations of the units in the *Obstacle Feedback Module.* These are: without any feedback as a baseline (BL), with only virtual fixture (VF), with only vibrotactile warning (VW), and with the combined use of virtual fixture and vibrotactile warning (VF + VW). Before the experiments, a familiarization phase was carried out separately for the virtual fixture and vibrotactile warning feedback modalities. This phase continued until the subjects felt comfortable with

these modalities, and they were informed that there could be different combinations of these during the experiments.

To prevent the subjects from learning the obstacle positions, we designed 4 different scenarios with varied obstacle placements. The visual representation of these scenarios can be found in Fig. 4. In each of the scenarios, the obstacles were strategically placed in locations where they were not initially visible to the human and remained occluded for the majority of the experiment. It should be noted that each scenario includes an obstacle positioned directly behind the robot base, creating a situation where a collision would occur before they reached the target line. Once the obstacles were placed, the participants were instructed to reach the finish line by taking the shortest path possible while maintaining a comfortable distance from the obstacles around.

The experiments were conducted with 8 female and 8 male (age: 26.8 $\pm$ 6.7 years; mass: 64.9 $\pm$ 16.2 kg; height: 172.4 $\pm$ 10.1 cm)[3] volunteers in accordance with the Declaration of Helsinki, and the protocol was approved by the ethics committee Azienda Sanitaria Locale (ASL) Genovese N.3 (Protocol IIT_HRII_ERGOLEAN 156/2020). Each participant performed the co-transportation experiment 4 times. In these trials, all the feedback modalities and the designed scenarios were executed randomly, one for each. In total, each feedback modality was tested 16 times across all four scenarios. Additionally, to eliminate the learning effect between trials, the order of the experiments was arranged in a way that in each trial order, all feedback modalities and scenarios were carried out 4 times.

4.3. Performance Metrics and Assessment Tools

At the end of each trial, the participants were asked to complete two questionnaires: NASA-TLX (NASA Task Load Index) [62] and SUS (System Usability Scale) [63]. These questionnaires were used to rate the qualitative aspects of the participant's experience for each feedback modality employed during the experiments. While the NASA-TLX assesses participants' perceived workload and task difficulty, the SUS evaluates the user-friendliness and usability of the modalities. In addition to these qualitative questionnaires, the following metrics are formulated for the quantitative analysis of task-related performance:

- **Success Rate (SR)**: It indicates the percentage of trials where participants reached the target line without having collisions with obstacles.
- **Completion Time (CT)**: The total time from the beginning of the co-carry task to the end is recorded for each trial. Notice that this metric is calculated only when the human-robot team did not collide with the obstacle.
- **Trajectory Length (TL)**: This is the total distance covered by the participants while reaching the target line. In order to compute this metric, we utilized the position data of the mobile base since the human and the robot were rigidly connected during the experiments. Similar to the previous metric, this one is also calculated only when the trial is considered successful.
- **Virtual Fixture Activation (VFA)**: This metric is formulated to calculate the activation percentage of the virtual fixture for each trial. It is computed as:

$$\mathbf{VFA} = \frac{\int_{t_s}^{t_e} \beta(t)dt}{t_e - t_s}, \tag{22}$$

where t_s and t_e are the starting and ending times of the experiment, and β is a step function that indicates the virtual fixture activation (see Eq. 17).

5. RESULTS AND DISCUSSION

Fig. 4 depicts the experimental results for a single participant who carried out four randomized trials, as explained in Sec. 4.2. In this figure, the left column plots illustrate the paths of the mobile base until the participant reaches the finish line, along with the dimensions of the room in which the experiment was executed and the positions of the obstacles located in the environment. The corresponding plots on the right show the results collected from these trials. The performed trials with different feedback modalities are presented in the following order from top to bottom: Baseline (BL) with Scenario 3 (Fig. 4a), Virtual Fixture (VF) with Scenario 4 (Fig. 4b), Vibrotactile Warning (VW) with Scenario 1 (Fig. 4c), and the combined use of Virtual Fixture and Vibrotactile Warning (VF + VW) with Scenario 2 (Fig. 4d).

During the BL trial, the participant directly proceeded with a forward movement toward the finished line, aligning with the goal of minimizing the trajectory length (see Fig. 4a). However, the trial could not be completed because of the collision. This indicates that the participant was unable to see the obstacle as it was occluded by the object being carried.

On the other hand, in the second trial, the participant could successfully finish the task where the VF feedback modality was available (see Fig. 4b). Thanks to the virtual fixture, the intended movement of the participant towards the obstacles was constrained to avoid collisions when the human-robot dyad was critically close to them. During the brief period indicated by the shaded area A in Fig. 4b3, it can be seen how the virtual fixture starts to operate. Here, the value of b (Eq. 15), which indicates the activation of the virtual fixture, goes to 1, leading to the filtering of the desired velocity towards the obstacle (see v_x tends to 0). Following this, despite the participant's continuous attempts to move directly in the X direction that may cause potential collisions (see increase in F_x in Fig. 4b1), the robot remained stationary. When the participant started to apply the forces to switch the motion direction to the left, the b value tends to 0 to allow movement (see highlighted area B in Fig. 4b3). Finally, the participant successfully reached the target line by

[3] Subject data is reported as: mean $\pm$ standard deviation.

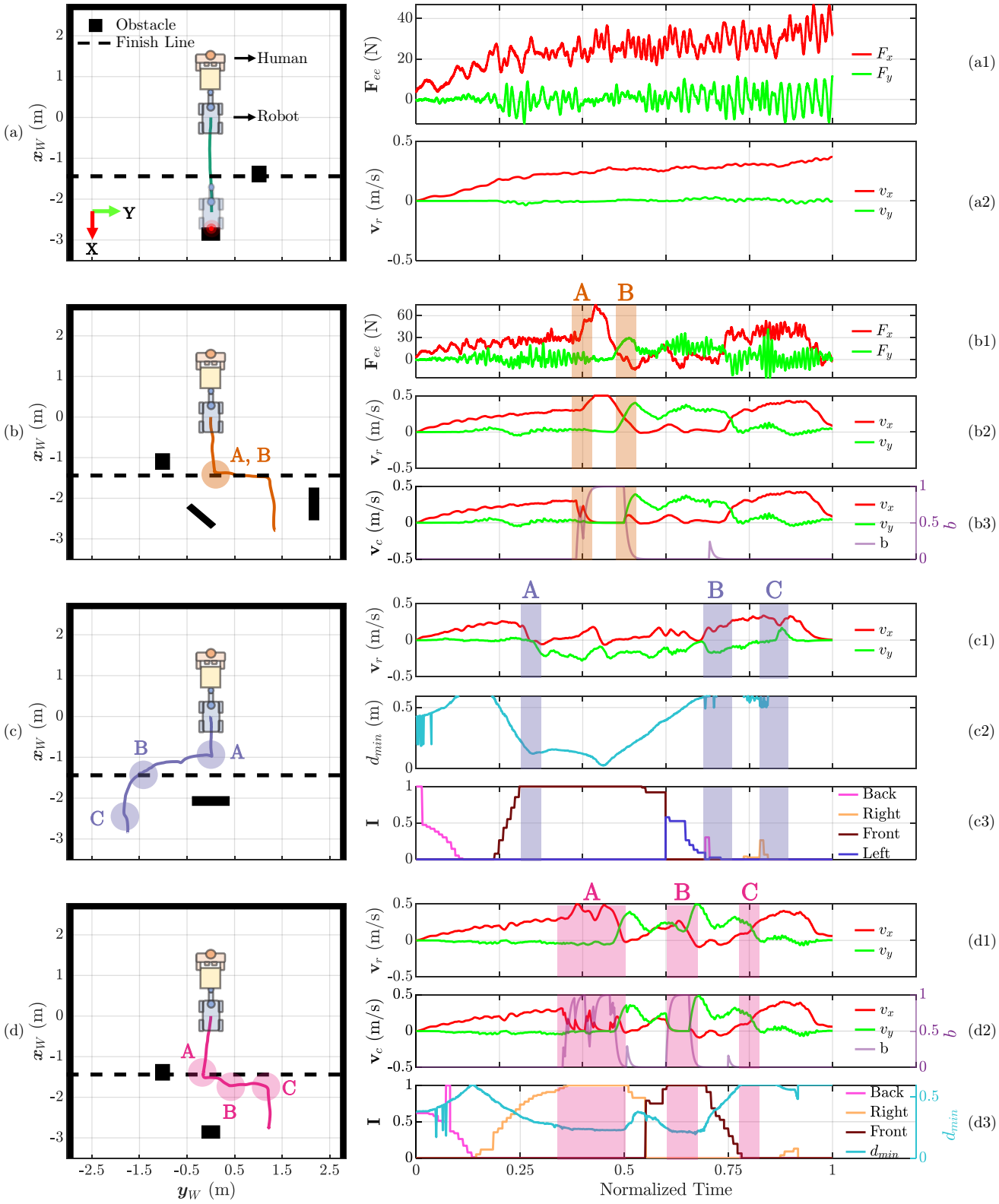

Fig. 4: Results of the experiments of a single participant. The plots illustrate the trials with (a) Baseline (BL) with Scenario 3, (b) Virtual Fixture (VF) with Scenario 4, (c) Vibrotactile Warning (VW) with Scenario 1, and (d) the combined use of Virtual Fixture and Vibrotactile Warning (VF + VW) with Scenario 2. While the left column plots display the paths of the mobile platform as the participant navigates towards the finish line, along with the positions of the obstacles located in the environment. The corresponding plots on the right present the results collected from these trials.

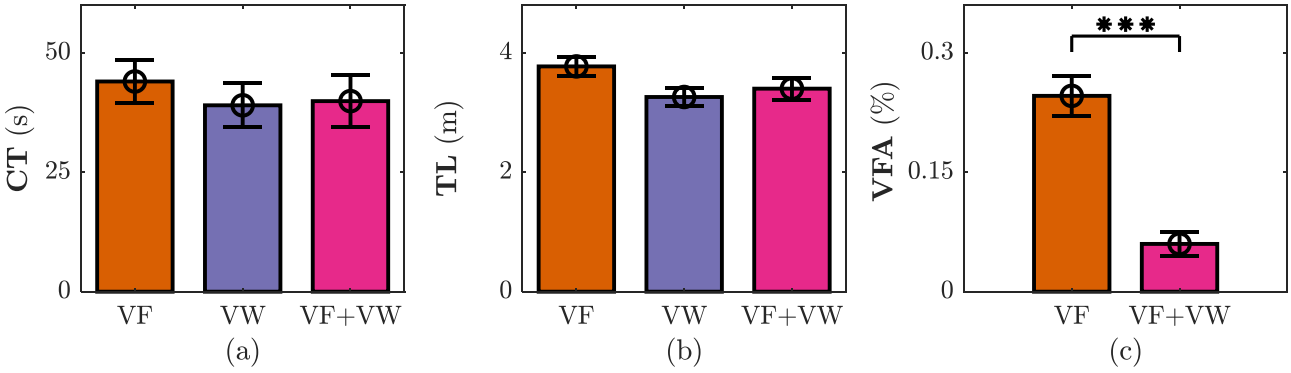

Fig. 5: The means and the standard errors of the performance metrics for the feedback modalities considering the successful trials. In addition, the outcomes of the sign-test conducted between the VF and VF+VW are reported where *** indicates $p < 0.001$.

readjusting the route to the front after maintaining a sideway motion until moving away from the obstacle.

At the beginning of the third trial, the participant experienced the vibration stimuli due to close proximity to the wall behind (see Fig. 4c3). As the participant proceeded with forward motion, the intensity of this vibration decreased. Subsequently, the vibrated region altered to the front and increased as the robot approached the obstacle. When the intensity reached its maximum, indicating that there exists a very close obstacle behind the robot, the participant changed the motion by moving to the right (see highlighted area A in Fig. 4c1). During this sideways movement with a slight forward component, the vibration region shifted to the left, providing information that the object was no longer behind the robot. When the intensity of this vibration decreased, the participant started to follow a more direct route toward the finish line (see highlighted area B in Fig. 4c1). The experiment was completed successfully with a small adjustment to the left at the end since ErgoTac-Belt generated feedback regarding the wall on the right (see highlighted area B in Fig. 4c3).

In the final trial, the participant reached the target line without having any collision, thanks to VF and VW feedback modalities. After a slightly deviated forward movement to the right at the beginning of the trial, the virtual fixture became active due to the obstacle on the right illustrated by the shaded area A in Fig. 4d2. Since the vibrotactile stimuli warned the participant about the obstacle on the right, the participant decided to move to the left when the virtual fixture constrained the motion. Following a small sideway movement, the participant decided to move diagonally towards the finish line. However, the virtual fixture and vibrotactile warning indicated the obstacle behind the robot, resulting in the continuation of the sideway motion (see highlighted area B in Fig. 4d2, Fig. 4d3)). When the front ErgoTac device stopped vibrating, the participant finished the experiment by going directly to the finish line (see highlighted area B in Fig. 4d3).

Table 2
Success Rate of the feedback modalities with the designed scenarios

	S1	S2	S3	S4	
Baseline (BL)	0/4	0/4	0/4	0/4	0%
Virtual Fixture (VF)	4/4	4/4	4/4	4/4	100%
Vibrotactile Warning (VW)	4/4	2/4	3/4	3/4	75%
VF+VW	4/4	4/4	4/4	4/4	100%

The success rate of the feedback modalities during the designed scenarios is reported for all participants in Table 2. As anticipated, none of the participants were able to complete the task without any feedback (BL). On the other hand, when the virtual fixture was employed (VF or VF+VW), all the participants reached the finish line without experiencing any collisions. This result is aligned with the evidence that the virtual fixture effectively prevents collisions with the environment. As previously explained, although the vibrotactile warning assists the participants by informing them about the object's location, it may not entirely avoid collisions. Indeed, four participants could not finish the trial due to collisions where only vibrotactile warning feedback was available.

Fig. 5 displays the means and the standard errors of the remaining performance metrics described in Sec. 4.3. These results were calculated based on the successful trials of the participants, which consisted of 16 trials for VF and VF+VW and 12 trials for VW. Given the difference in the number of successful trials for VW, we conducted the sign-test only between VF and VF+VW. As can be seen from Fig. 5a, the mean completion time is the highest for VF among the feedback modalities, whereas VW has the lowest one. However, no statistically significant difference is observed between VF and VF+VW. When the trajectory length results are analyzed (see Fig. 5b), similar patterns to the completion time emerge, with VF having the longest mean trajectory and the shortest mean trajectory being achieved with VW. Furthermore, there is no statistically significant difference between VF and VF+VW. These results can be explained as follows: When only the VF feedback modality

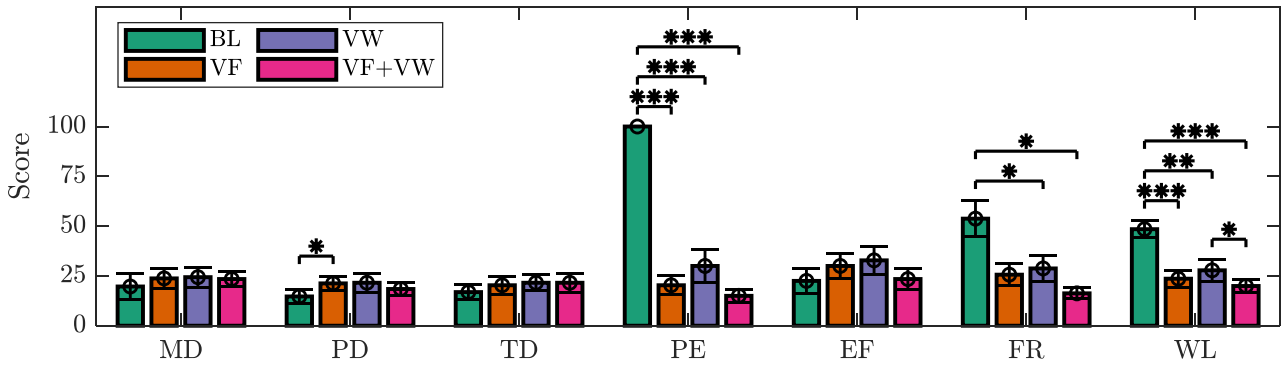

Fig. 6: The means and the standard errors obtained from the NASA-TLX questionnaires for the feedback modalities along with the outcomes of the sign-test carried out: *: $p < 0.05$, **: $p < 0.01$, ***: $p < 0.001$. (MD: Mental Demand, PD: Physical Demand, TD: Temporal Demand, PE: Performance, EF: Effort, FR: Frustration, WL: Overall Workload)

is employed, the participants tend to follow a longer trajectory due to deviations from the shortest path while trying to comprehend the location of the obstacles. On the other hand, as a result of the valuable information that vibrotactile warning provides about the environment, it allows participants to make more informed and efficient decisions during navigation. The statistically significant decrease ($p < 0.001$) in virtual fixture activation when the virtual fixture was combined with vibrotactile warning further supports this argument (see Fig. 5c). The presence of the vibrotactile warning before the human-robot team approached the obstacle closely enough to activate the virtual fixture allowed the participants to avoid obstacles more efficiently.

The qualitative results obtained from the NASA-TLX questionnaire, which consist of the participants' scores for their perceived workload across six subscales and the computed overall workload, are presented in Fig. 6. In this figure, the means and standard errors for all the questionnaire categories of the feedback modalities are represented as bar plots, along with the outcomes of the sign-tests. Because none of the participants achieved to reach the target line with the BL feedback modality, all of them rated a score of 100 for the Performance category, representing the lowest possible score in NASA-TLX. For this category, the remaining feedback modalities demonstrate significantly superior scores compared to the BL ($p < 0.001$). Moreover, the participants perceived significantly higher frustration during BL experiments than VW and VF+VW ($p < 0.05$). On the other hand, BL has the minimum mean for the Physical Demand category, which is significantly different from VF ($p < 0.05$). This is because participants tried to complete the task with direct forward movement without any feedback, and the experiment stopped early when they hit the obstacles. However, completing the task is more physically demanding during VF trials due to adjustments required in case the virtual fixture is active. When the overall workload results are analyzed, it can be seen that the participants favored having feedback about the obstacles located in the environment during the co-transportation task, indicated by the statistically significant differences between BL and the other feedback modalities. The minimum mean for the workload is obtained with VF+VW, which has significantly superior scores compared to VW.

The result of the SUS questionnaire reported in Fig. 7 shows that the average score of BL was significantly lower than the other feedback modalities. Besides, the participants favored the combination of the two feedback units most, while all feedback modalities except BL were categorized as highly acceptable. Additionally, because the score of BL is below the usability limit [64], this modality is considered unacceptable for use, given the fact that none of the participants were able to complete the co-carrying task without any feedback.

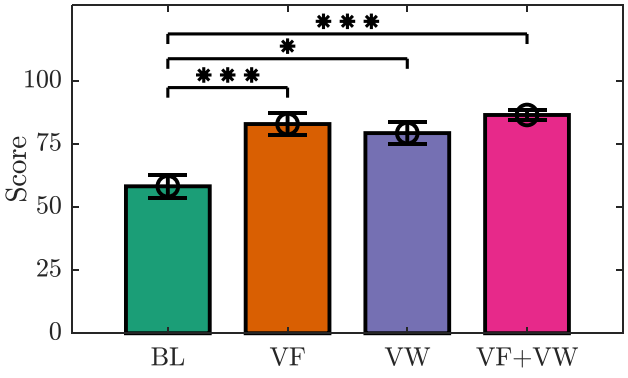

Fig. 7: The means and the standard errors obtained from the SUS questionnaires for the feedback modalities along with the outcomes of the sign-test carried out: *: $p < 0.05$, ***: $p < 0.001$.

It is important to note that the proposed method is not restricted to any particular task. For any task involving physical interaction between the mobile platform and humans, the proposed method can be employed to ensure the human-robot team avoids collision with surroundings by providing warnings about the proximity of the obstacles. For example, the proposed method can be integrated into a robotic walking support system [65], or applied to entertainment tasks such as human-robot dancing [66, 67].

In order to employ our situational awareness framework in the practical use cases mentioned above, it is necessary to identify its current limitations. In our framework, the human and the robot are enclosed within a capsule, assuming they initially face each other and maintain their respective positions while jointly transporting the object in between. However, certain manipulation tasks can be carried out more easily and effectively when the operator has the flexibility to adopt various configurations relative to the robot during co-carrying. Moreover, when we consider the drawbacks of the robot's sensory system, the incorporated Lidars limit the perception into a 2D plane. Despite Lidars being less affected by environmental conditions such as weather and changes in light compared to other vision-based sensors, the inherent challenge linked to this technology is the existence of excessive reflections in the surroundings. These reflections can elevate the noise level, potentially leading to false activation of VF and VW modules. Nevertheless, we did not have any noise-related issues in the Lidar's 2D scan during our experiments, as expected, since this limitation may emerge in environmental conditions that are far from ideal. Additionally, denoising Lidar noise has been extensively explored in the literature [68], thus there are various techniques available to overcome this limitation when it emerges.

6. CONCLUSION

In this article, we have proposed a human-robot collaborative transportation framework that includes as a main novelty a multi-modal haptic feedback module that informs the human operator of the presence of obstacles in the environment by augmenting their sensory capabilities with the robot's sensory system. The module integrates a haptic feedback unit at the cutaneous level thanks to four vibrotactile devices placed in a belt on the subject's body and a unit that acts at the kinesthetic level through virtual fixtures. The latter incorporates an additional safety layer as it not only warns the user but also prevents the robot from coming into contact with obstacles. The manuscript has described in detail the functionality of both systems, as well as their integration within the robot controller and sensory system in our previously developed feedback-less co-transportation framework. Experiments have been carried out, allowing an objective evaluation thanks to quantitative metrics and subjective evaluations based on the user-level experiences of 16 participants who have tested the system in a real industrial-like environment. In addition, a comparative analysis of both haptic feedback modalities and a statistical analysis has also been conducted to establish which modality is the desired one based on several factors.

The outcomes of this work conclude that this new module improves the situational awareness of the human operator. The experimental evaluation results with non-expert subjects indicated that the haptic feedback provided by the module enabled the human partner to perform a co-transport task even in extreme situations where the operator's field of view is highly compromised. Thus, it improved the human-robot team's safety allowing the human operator to command the team in an unknown environment with unknown and hidden obstacles. Furthermore, the study concludes that integrating both haptic feedback modalities is the best solution and is preferred by the participants.

In the future, we plan to focus on investigating and implementing potential solutions to address the existing limitations previously discussed in Sec. 5. For instance, a human leg-tracker module can be developed and incorporated with the proposed framework to dynamically reconfigure the relative position of the human with respect to the robot in real-time. Furthermore, a natural extension for our perception module could be the integration of the 3D Lidar system. This integration will allow us to adjust the controller parameters on the fly to prioritize the movement to the arm or the base taking into account the 3D mapping of the obstacle.

A. ACKNOWLEDGEMENT

This work was supported in part by the ERC-StG Ergo-Lean (Grant Agreement No.850932), by the European Union's Horizon 2020 research and innovation programme SOPHIA (Grant Agreement No. 871237) and CONCERT (Grant Agreement No. 101016007).

References

[1] Arash Ajoudani, Andrea Maria Zanchettin, Serena Ivaldi, Alin Albu-Schäffer, Kazuhiro Kosuge, and Oussama Khatib. Progress and prospects of the human–robot collaboration. *Autonomous Robots*, 42 (5):957–975, 2018.

[2] J. Krüger, T.K. Lien, and A. Verl. Cooperation of human and machines in assembly lines. *CIRP Annals*, 58(2):628–646, 2009. ISSN 0007-8506. doi: https://doi.org/10.1016/j.cirp.2009.09.009.

[3] J. Ernesto Solanes, Luis Gracia, Pau Muñoz-Benavent, Jaime Valls Miro, Vicent Girbés, and Josep Tornero. Human-robot cooperation for robust surface treatment using non-conventional sliding mode control. *ISA Transactions*, 80:528–541, 2018. ISSN 0019-0578. doi: https://doi.org/10.1016/j.isatra.2018.05.013.

[4] Luka Peternel, Nikos Tsagarakis, Darwin Caldwell, and Arash Ajoudani. Robot adaptation to human physical fatigue in human–robot co-manipulation. *Autonomous Robots*, 42:1–11, 06 2018. doi: 10.1007/s10514-017-9678-1.

[5] J.L. Drury, J. Scholtz, and H.A. Yanco. Awareness in human-robot interactions. In *SMC'03 Conference Proceedings. 2003 IEEE International Conference on Systems, Man and Cybernetics. Conference Theme - System Security and Assurance (Cat. No.03CH37483)*, volume 1, pages 912–918, 2003. doi: 10.1109/ICSMC.2003.1243931.

[6] Yusuf Aydin, Doganay Sirintuna, and Cagatay Basdogan. Towards collaborative drilling with a cobot using admittance controller. *Transactions of the Institute of Measurement and Control*, 43(8):1760–1773, 2021. doi: 10.1177/0142331220934643.

[7] Doganay Sirintuna, Idil Ozdamar, Yusuf Aydin, and Cagatay Basdogan. Detecting human motion intention during phri using artificial neural networks trained by emg signals. In *2020 29th IEEE International Conference on Robot and Human Interactive Communication (RO-MAN)*, pages 1280–1287, 2020. doi: 10.1109/RO-MAN47096.2020.9223438.

[8] Ramsundar Kalpagam Ganesan, Yash K Rathore, Heather M Ross, and Heni Ben Amor. Better teaming through visual cues: how projecting imagery in a workspace can improve human-robot collaboration. *IEEE Robotics & Automation Magazine*, 25(2):59–71, 2018.

[9] Idil Ozdamar, Marco Laghi, Giorgio Grioli, Arash Ajoudani, Manuel G. Catalano, and Antonio Bicchi. A shared autonomy reconfigurable control framework for telemanipulation of multi-arm systems. *IEEE Robotics and Automation Letters*, 7(4):9937–9944, 2022. doi: 10.1109/LRA.2022.3191200.

[10] Elena Merlo, Edoardo Lamon, Fabio Fusaro, Marta Lorenzini, Alessandro Carfi, Fulvio Mastrogiovanni, and Arash Ajoudani. Dynamic human-robot role allocation based on human ergonomics risk prediction and robot actions adaptation. In *2022 International Conference on Robotics and Automation (ICRA)*, pages 2825–2831. IEEE, 2022.

[11] Aaron St. Clair and Maja Mataric. How robot verbal feedback can improve team performance in human-robot task collaborations. In *Proceedings of the Tenth Annual ACM/IEEE International Conference on Human-Robot Interaction*, HRI '15, page 213–220, New York, NY, USA, 2015. Association for Computing Machinery. ISBN 9781450328838. doi: 10.1145/2696454.2696491.

[12] Doganay Sirintuna, Idil Ozdamar, and Arash Ajoudani. Carrying the uncarriable: a deformation-agnostic and human-cooperative framework for unwieldy objects using multiple robots. In *2023 IEEE International Conference on Robotics and Automation (ICRA)*, pages 7497–7503, 2023. doi: 10.1109/ICRA48891.2023.10160677.

[13] Marta Lorenzini, Juan M. Gandarias, Luca Fortini, Wansoo Kim, and Arash Ajoudani. Ergotac-belt: Anticipatory vibrotactile feedback to lead centre of pressure during walking. In *2022 9th IEEE RAS/EMBS International Conference for Biomedical Robotics and Biomechatronics (BioRob)*, page 01–06. IEEE Press, 2022. doi: 10.1109/BioRob52689.2022.9925563.

[14] Leonel Rozo, Sylvain Calinon, Darwin G. Caldwell, Pablo Jiménez, and Carme Torras. Learning physical collaborative robot behaviors from human demonstrations. *IEEE Transactions on Robotics*, 32(3): 513–527, 2016. doi: 10.1109/TRO.2016.2540623.

[15] Paul Evrard, Elena Gribovskaya, Sylvain Calinon, Aude Billard, and Abderrahmane Kheddar. Teaching physical collaborative tasks: Object-lifting case study with a humanoid. In *2009 9th IEEE-RAS International Conference on Humanoid Robots*, pages 399–404. IEEE, 2009.

[16] Antoine Bussy, Pierre Gergondet, Abderrahmane Kheddar, François Keith, and André Crosnier. Proactive behavior of a humanoid robot in a haptic transportation task with a human partner. In *2012 IEEE RO-MAN: The 21st IEEE International Symposium on Robot and Human Interactive Communication*, pages 962–967. IEEE, 2012.

[17] Antoine Bussy, Abderrahmane Kheddar, André Crosnier, and François Keith. Human-humanoid haptic joint object transportation case study. In *2012 IEEE/RSJ International Conference on Intelligent Robots and Systems*, pages 3633–3638, 2012. doi: 10.1109/IROS.2012.6385921.

[18] Don Joven Agravante, Andrea Cherubini, Antoine Bussy, Pierre Gergondet, and Abderrahmane Kheddar. Collaborative human-humanoid carrying using vision and haptic sensing. In *2014 IEEE International Conference on Robotics and Automation (ICRA)*, pages 607–612, 2014. doi: 10.1109/ICRA.2014.6906917.

[19] Alexander Mörtl, Martin Lawitzky, Ayse Kucukyilmaz, Metin Sezgin, Cagatay Basdogan, and Sandra Hirche. The role of roles: Physical cooperation between humans and robots. *The International Journal of Robotics Research*, 31(13):1656–1674, 2012. doi: 10.1177/0278364912455366.

[20] Vincent Duchaine and Clement M. Gosselin. General model of human-robot cooperation using a novel velocity based variable impedance control. In *Second Joint EuroHaptics Conference and Symposium on Haptic Interfaces for Virtual Environment and Teleoperator Systems (WHC'07)*, pages 446–451, 2007. doi: 10.1109/WHC.2007.59.

[21] Vincent Duchaine and Clément Gosselin. Safe, stable and intuitive control for physical human-robot interaction. In *2009 IEEE International Conference on Robotics and Automation*, pages 3383–3388. IEEE, 2009.

[22] Jörg Stückler and Sven Behnke. Following human guidance to cooperatively carry a large object. In *2011 11th IEEE-RAS International Conference on Humanoid Robots*, pages 218–223, 2011. doi: 10.1109/Humanoids.2011.6100917.

[23] Doganay Sirintuna, Alberto Giammarino, and Arash Ajoudani. An object deformation-agnostic framework for human–robot collaborative transportation. *IEEE Transactions on Automation Science and Engineering*, pages 1–14, 2023. doi: 10.1109/TASE.2023.3259162.

[24] Louis B Rosenberg. The use of virtual fixtures as perceptual overlays to enhance operator performance in remote environments. Technical report, Stanford Univ Ca Center for Design Research, 1992.

[25] Louis B Rosenberg. Virtual fixtures: Perceptual tools for telerobotic manipulation. In *Proceedings of IEEE virtual reality annual international symposium*, pages 76–82. Ieee, 1993.

[26] Bruno Siciliano, Oussama Khatib, and Torsten Kröger. *Springer handbook of robotics*, volume 200. Springer, 2008.

[27] Stuart A Bowyer, Brian L Davies, and Ferdinando Rodriguez y Baena. Active constraints/virtual fixtures: A survey. *IEEE Transactions on Robotics*, 30(1):138–157, 2013.

[28] Murilo M Marinho, Hisashi Ishida, Kanako Harada, Kyoichi Deie, and Mamoru Mitsuishi. Virtual fixture assistance for suturing in robot-aided pediatric endoscopic surgery. *IEEE Robotics and Automation Letters*, 5(2):524–531, 2020.

[29] Murilo M Marinho, Bruno V Adorno, Kanako Harada, Kyoichi Deie, Anton Deguet, Peter Kazanzides, Russell H Taylor, and Mamoru Mitsuishi. A unified framework for the teleoperation of surgical robots in constrained workspaces. In *2019 international conference on robotics and automation (ICRA)*, pages 2721–2727. IEEE, 2019.

[30] Stuart A Bowyer and Ferdinando Rodriguez y Baena. Dissipative control for physical human–robot interaction. *IEEE Transactions on Robotics*, 31(6):1281–1293, 2015.

[31] Catherina Burghart, Jochen Keitel, Stefan Hassfeld, Ulrich Rembold, and Heinz Woern. Robot controlled osteotomy in craniofacial surgery. In *First International Workshop on Haptic Devices in Medical Applications Proceedings*, pages 12–22. Citeseer, 1999.

[32] Alessandro Bettini, Panadda Marayong, Samuel Lang, Allison M Okamura, and Gregory D Hager. Vision-assisted control for manipulation using virtual fixtures. *IEEE Transactions on Robotics*, 20(6): 953–966, 2004.

[33] O Khatib and J Le Maitre. Dynamic control of manipulators operating in a complex environment. In *On Theory and Practice of Robots and Manipulators, 3rd CISM-IFToMM Symp*, volume 267, 1978.

[34] Mario Selvaggio, Fei Chen, Boyang Gao, Gennaro Notomista, Francesco Trapani, and Darwin Caldwell. Vision based virtual fixture generation for teleoperated robotic manipulation. In *2016 International Conference on Advanced Robotics and Mechatronics (ICARM)*, pages 190–195. IEEE, 2016.

[35] Jing Luo, Zhidong Lin, Yanan Li, and Chenguang Yang. A teleoperation framework for mobile robots based on shared control. *IEEE Robotics and Automation Letters*, 5(2):377–384, 2019.

[36] Theodora Kastritsi, Iason Sarantopoulos, Sotiris Stavridis, Dimitrios Papageorgiou, and Zoe Doulgeri. Manipulation of a whole surgical tool within safe regions utilizing barrier artificial potentials. In Jorge Henriques, Nuno Neves, and Paulo de Carvalho, editors, *XV Mediterranean Conference on Medical and Biological Engineering and Computing – MEDICON 2019*, pages 1559–1570, Cham, 2020. Springer International Publishing. ISBN 978-3-030-31635-8.

[37] Theodora Kastritsi, Dimitrios Papageorgiou, Iason Sarantopoulos, Sotiris Stavridis, Zoe Doulgeri, and George A. Rovithakis. Guaranteed active constraints enforcement on point cloud-approximated regions for surgical applications. In *2019 International Conference on Robotics and Automation (ICRA)*, pages 8346–8352, 2019. doi: 10.1109/ICRA.2019.8793953.

[38] Matteo Melchiorre, Laura Salamina, Leonardo Sabatino Scimmi, Stefano Mauro, and Stefano Pastorelli. Experiments on the artificial potential field with local attractors for mobile robot navigation. *Robotics*, 12(3):81, 2023.

[39] Chau Ton, Zhen Kan, and Siddhartha S Mehta. Obstacle avoidance control of a human-in-the-loop mobile robot system using harmonic potential fields. *Robotica*, 36(4):463–483, 2018.

[40] Xuzhong Yan, Heng Li, Angus R Li, and Hong Zhang. Wearable IMU-based real-time motion warning system for construction workers' musculoskeletal disorders prevention. *Automation in Construction*, 74:2–11, 2017.

[41] Nicolas Vignais, Markus Miezal, Gabriele Bleser, Katharina Mura, Dominic Gorecky, and Frédéric Marin. Innovative system for real-time ergonomic feedback in industrial manufacturing. *Applied ergonomics*, 44(4):566–574, 2013.

[42] Stephen Bevan. Economic impact of musculoskeletal disorders (MSDs) on work in Europe. *Best Practice & Research Clinical Rheumatology*, 29(3):356–373, 2015.

[43] Wansoo Kim, Marta Lorenzini, Pietro Balatti, Phuong D.H. Nguyen, Ugo Pattacini, Vadim Tikhanoff, Luka Peternel, Claudio Fantacci, Lorenzo Natale, Giorgio Metta, and Arash Ajoudani. Adaptable workstations for human-robot collaboration: A reconfigurable framework for improving worker ergonomics and productivity. *IEEE Robotics & Automation Magazine*, 26(3):14–26, 2019.

[44] Ying Zhang, Terrence Fernando, Hannan Xiao, and Adrian R L Travis. Evaluation of auditory and visual feedback on task performance in a virtual assembly environment. *Presence: Teleoperators and Virtual Environments*, 15(6):613–626, 2006.

[45] David T Goomas and Paul HP Yeow. Ergonomics improvement in a harsh environment using an audio feedback system. *International Journal of Industrial Ergonomics*, 40(6):767–774, 2010.

[46] Richard E Fan, Martin O Culjat, Chih-Hung King, Miguel L Franco, Richard Boryk, James W Bisley, Erik Dutson, and Warren S Grundfest. A haptic feedback system for lower-limb prostheses. *IEEE Transactions on Neural Systems and Rehabilitation Engineering*, 16 (3):270–277, 2008.

[47] Arash Ajoudani, Sasha B Godfrey, Matteo Bianchi, Manuel G Catalano, Giorgio Grioli, Nikos Tsagarakis, and Antonio Bicchi. Exploring teleimpedance and tactile feedback for intuitive control of the pisa/iit softhand. *IEEE Transactions on Haptics*, 7(2):203–215, 2014.

[48] Aruni Upeksha Alahakone and SMN Arosha Senanayake. Vibrotactile feedback systems: Current trends in rehabilitation, sports and information display. In *IEEE/ASME International Conference on Advanced Intelligent Mechatronics*, pages 1148–1153, 2009.

[49] Andrea Casalino, Costanza Messeri, Maria Pozzi, Andrea Maria Zanchettin, Paolo Rocco, and Domenico Prattichizzo. Operator awareness in human–robot collaboration through wearable vibrotactile feedback. *IEEE Robotics and Automation Letters*, 3(4):4289–4296, 2018.

[50] Giulia Ballardini, Valeria Florio, Andrea Canessa, Giorgio Carlini, Pietro Morasso, and Maura Casadio. Vibrotactile feedback for improving standing balance. *Frontiers in Bioengineering and Biotechnology*, 8:94, 2020.

[51] Ying Zheng and John B Morrell. A vibrotactile feedback approach to posture guidance. In *IEEE Haptics Symposium*, pages 351–358. IEEE, 2010.

[52] Thomas Debus, Tae-Jeong Jang, Pierre Dupont, and Robert Howe. Multi-channel vibrotactile display for teleoperated assembly. In *Proceedings 2002 IEEE International Conference on Robotics and Automation (Cat. No. 02CH37292)*, volume 1, pages 592–597. IEEE, 2002.

[53] Wansoo Kim, Marta Lorenzini, Kağan Kapıcıoğlu, and Arash Ajoudani. Ergotac: A tactile feedback interface for improving human ergonomics in workplaces. *IEEE Robotics and Automation Letters*, 3 (4):4179–4186, 2018. doi: 10.1109/LRA.2018.2864356.

[54] Marta Lorenzini, Simone Ciotti, Juan M Gandarias, Simone Fani, Matteo Bianchi, and Arash Ajoudani. Performance analysis of vibrotactile and slide-and-squeeze haptic feedback devices for limbs postural adjustment. In *2022 31st IEEE International Conference on Robot and Human Interactive Communication (RO-MAN)*, pages 707–713. IEEE, 2022.

[55] Andrea Casalino, Costanza Messeri, Maria Pozzi, Andrea Maria Zanchettin, Paolo Rocco, and Domenico Prattichizzo. Operator awareness in human–robot collaboration through wearable vibrotactile feedback. *IEEE Robotics and Automation Letters*, 3(4):4289–4296, 2018. doi: 10.1109/LRA.2018.2865034.

[56] Theodora Kastritsi and Zoe Doulgeri. A passive admittance controller to enforce remote center of motion and tool spatial constraints with application in hands-on surgical procedures. *Robotics and Autonomous Systems*, 152:104073, 2022.

[57] Stefano Chiaverini, Olav Egeland, and Rakel K Kanestrom. Weighted damped least-squares in kinematic control of robotic manipulators. *Advanced robotics*, 7(3):201–218, 1992.

[58] Arati S Deo and Ian D Walker. Overview of damped least-squares methods for inverse kinematics of robot manipulators. *Journal of Intelligent and Robotic Systems*, 14(1):43–68, 1995.

[59] JOHNM Hollerbach and Ki Suh. Redundancy resolution of manipulators through torque optimization. *IEEE Journal on Robotics and Automation*, 3(4):308–316, 1987.

[60] Charles W Wampler. Manipulator inverse kinematic solutions based on vector formulations and damped least-squares methods. *IEEE Transactions on Systems, Man, and Cybernetics*, 16(1):93–101, 1986.

[61] Alberto Giammarino, Juan M. Gandarias, Pietro Balatti, Mattia Leonori, Marta Lorenzini, and Arash Ajoudani. Super-man: Supernumerary robotic bodies for physical assistance in human-robot conjoined actions, 2023.

[62] Sandra G. Hart and Lowell E. Staveland. Development of nasa-tlx (task load index): Results of empirical and theoretical research. In Peter A. Hancock and Najmedin Meshkati, editors, *Human Mental Workload*, volume 52 of *Advances in Psychology*, pages 139–183. North-Holland, 1988. doi: https://doi.org/10.1016/S0166-4115(08)62386-9.

[63] John Brooke. Sus: a "quick and dirty'usability. *Usability evaluation in industry*, 189(3):189–194, 1996.

[64] Aaron Bangor, Philip T. Kortum, and James T. Miller. An empirical evaluation of the system usability scale. *International Journal of Human–Computer Interaction*, 24(6):574–594, 2008.

[65] Oscar Chuy, Yasuhisa Hirata, and Kazuhiro Kosuge. A new control approach for a robotic walking support system in adapting user characteristics. *IEEE Transactions on Systems, Man, and Cybernetics, Part C (Applications and Reviews)*, 36(6):725–733, 2006.

[66] O Khatib, O Brock, K Yokoi, and R Holmberg. Dancing with juliet. In *Video Proc. of IEEE Int'l. Conf. on Robotics and Automation*, 1999.

[67] Takahiro Takeda, Yasuhisa Hirata, and Kazuhiro Kosuge. Dance partner robot cooperative motion generation with adjustable length of dance step stride based on physical interaction. In *2007 IEEE/RSJ International Conference on Intelligent Robots and Systems*, pages 3258–3263. IEEE, 2007.

[68] Luyao Zhang, Jianhua Chang, Hongxu Li, Zhen Xing Liu, Shuyi Zhang, and Rengxiang Mao. Noise reduction of lidar signal via local mean decomposition combined with improved thresholding method. *IEEE Access*, 8:113943–113952, 2020.